Electronic Supplementary Material (ESI) for Dalton Transactions.

Supporting Information for

Synthesis, structure, ultrafast kinetics, and light-induced dynamics of CuHETPHEN chromophores

Lars Kohler,[a] Dugan Hayes,[a] Jiyun Hong,[b] Tyler J. Carter,[a] Megan L. Shelby,[b] Kelly A. Fransted,[a] Lin X. Chen,[a,b] Karen L. Mulfort[a*]

[a]Division of Chemical Sciences and Engineering, Argonne National Laboratory, 9700 South Cass Avenue, Argonne IL 60439; [b]Department of Chemistry, Northwestern University, 2145 Sheridan Road, Evanston IL 60208

Crystal structure data for **3**.

Table S1. Details of crystal structure refinement of **3**

Formula	$C_{116}H_{103}Cu_2F_{12}N_8OP_2$
Mw (g mol^{-1})	2042.10
Lattice Type	Monoclinic
Space Group	P21n
a (Å)	18.3444(16)
b (Å)	40.808(4)
c (Å)	27.461(2)
α (°)	90.00
β (°)	96.3660(10)
γ (°)	90.00
V (Å^3)	20431(3)
Z	8
ρ_{calc} (g cm^{-1})	1.328
T (K)	100
λ (Å) [Mo kα]	0.71073
μ (mm^{-1})	0.524
S (GOF)	1.083
$R(F_o)$, $wR(F_o^2)$	0.10, 0.24

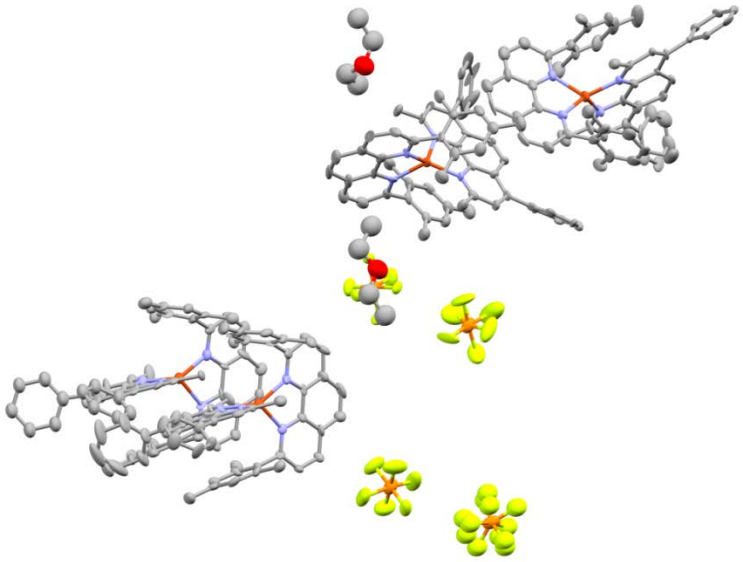

Figure S1. Asymmetric unit of the crystal structure of **3**. Ellipsoids represent 50% probability. Hydrogen atoms are omitted for clarity.

Room temperature emission spectra for **2**-**5**.

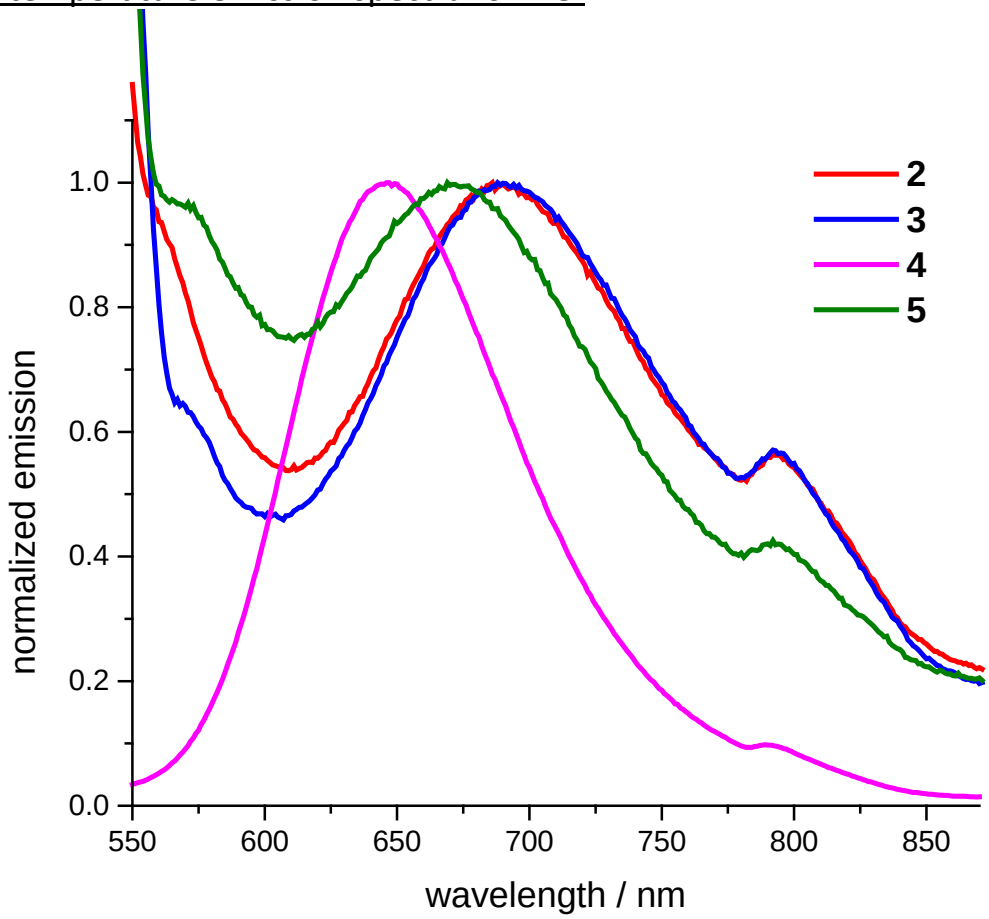

Figure S2. Room temperature emission spectra for **2**-**5** in dichloromethane, normalized at emission maximum. Excitation at MLCT absorbance maximum in dichloromethane:

2 460nm

3 469nm

4 442nm

5 468nm

Ultrafast transient optical spectra for **2**-**5** in acetonitrile.

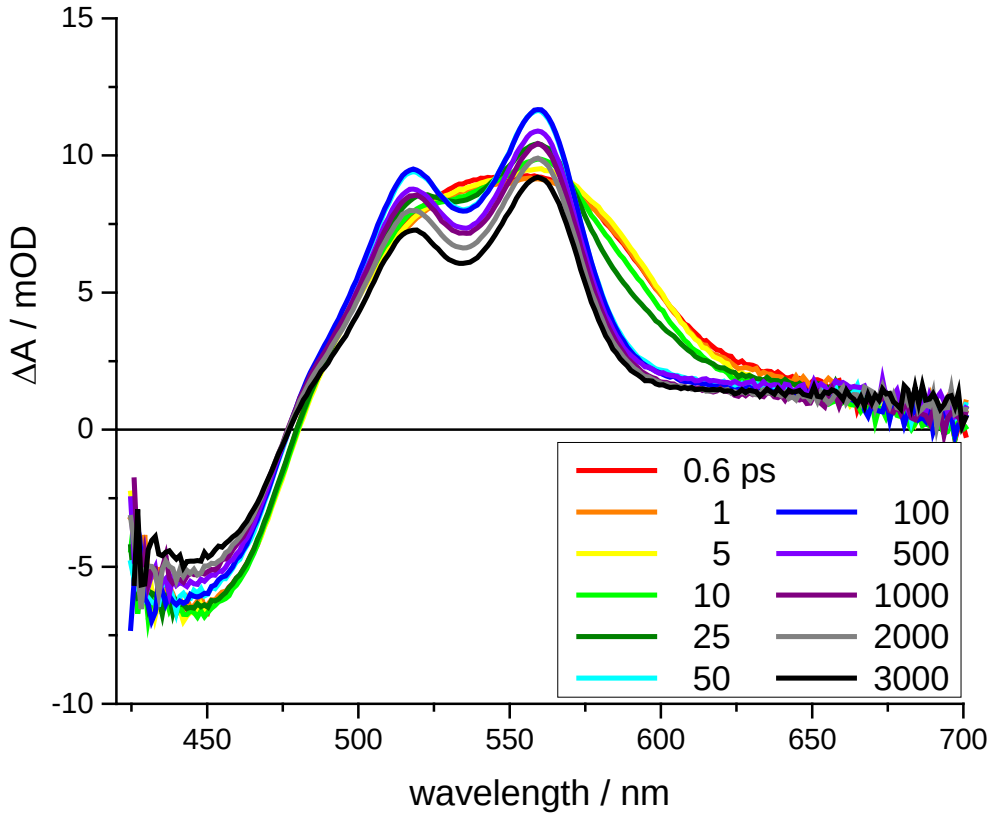

Figure S3. Transient optical spectra of **2** in acetonitrile following 415nm excitation.

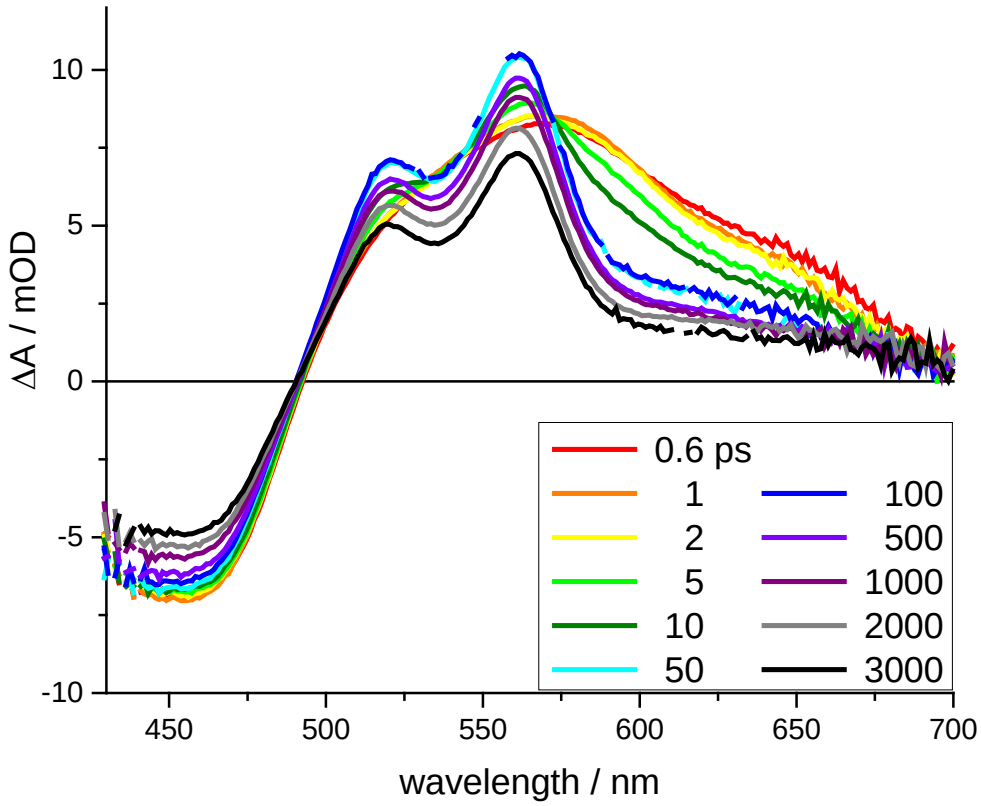

Figure S4. Transient optical spectra of **3** in acetonitrile following 415nm excitation.

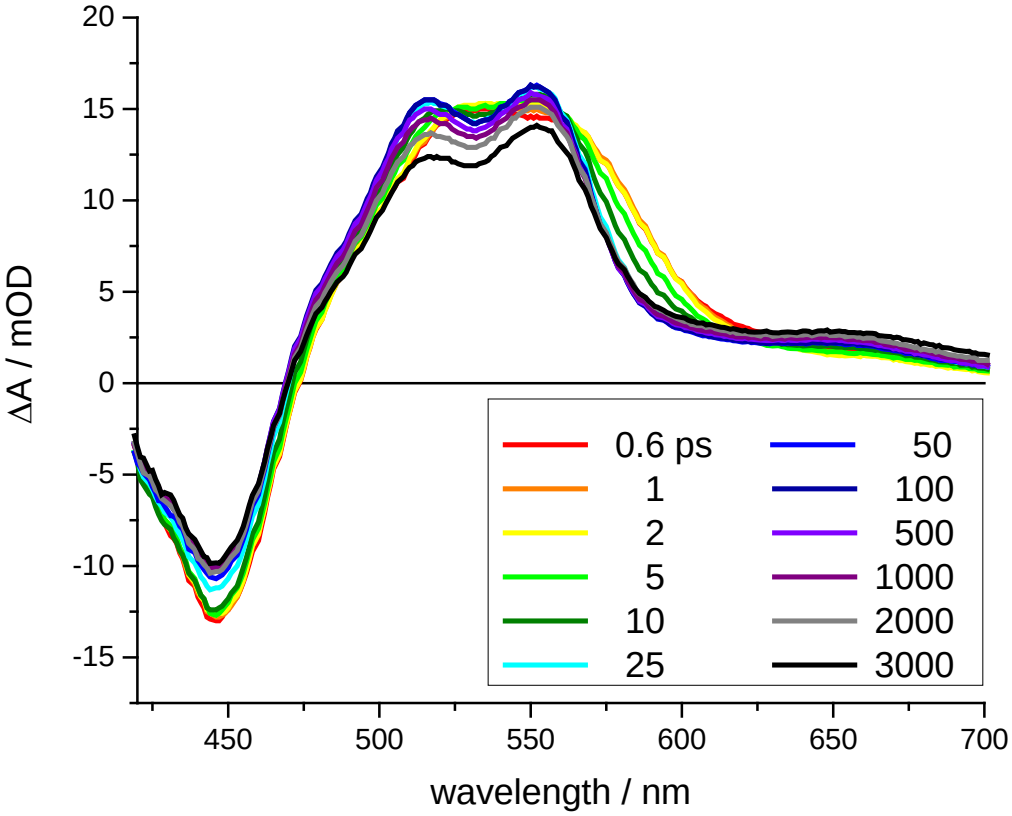

Figure S5. Transient optical spectra of **4** in acetonitrile following 415nm excitation.

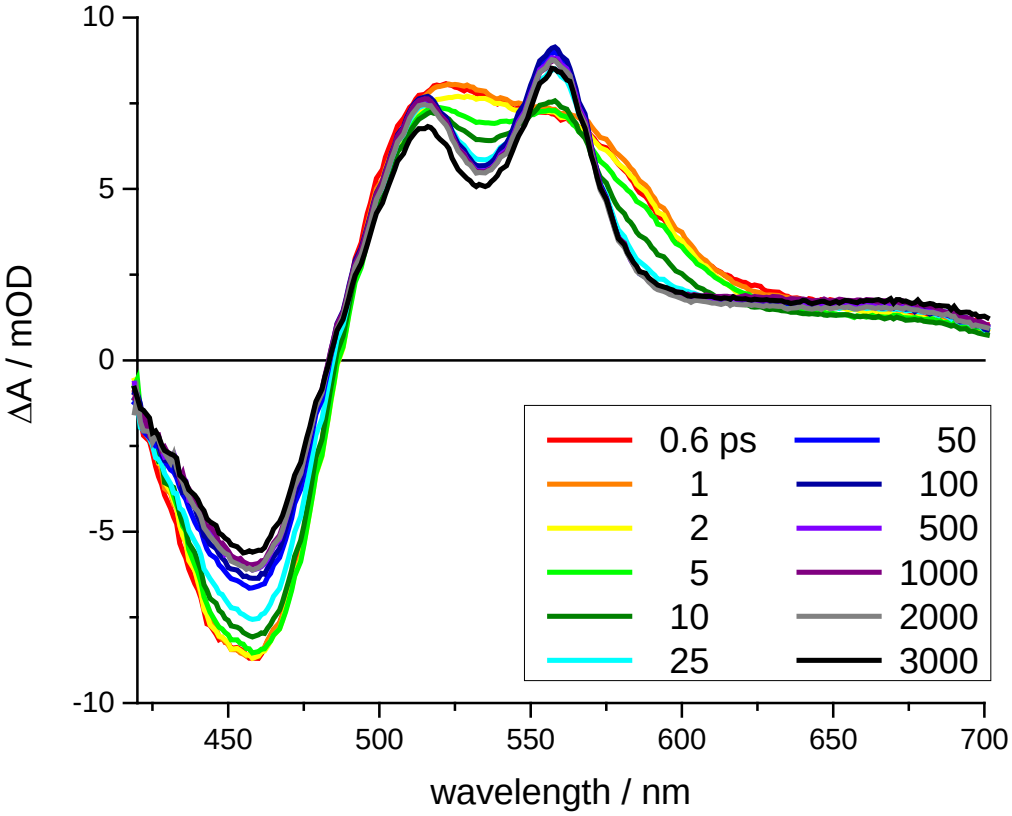

Figure S6. Transient optical spectra of **5** in acetonitrile following 415nm excitation.

Details of fitting ultrafast kinetics for **1**-**5**.

CuHETPHEN **1** in acetonitrile.
Given the significant difference in magnitude, the initial kinetics (τ_1, τ_2) and ^{3}MLCT decay (τ_3) were fit separately using a global multi-exponential decay routine over multiple wavelengths (noted below).

Determination of τ_1 and τ_2 for **1** was obtained using a bi-exponential decay fit to the kinetics at 533 and 557nm from 0.2-50ps:

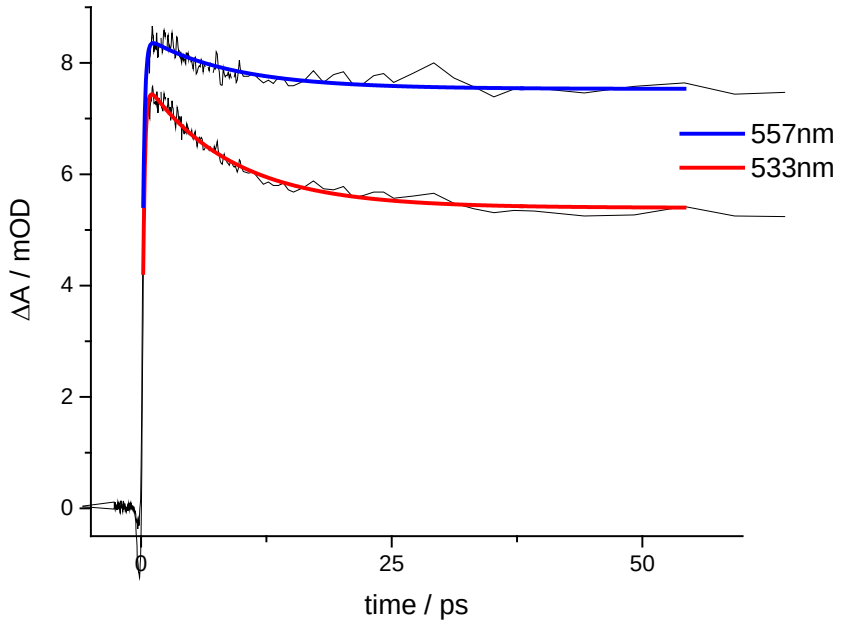

Figure S7. Global fit of early kinetics of **1** in acetonitrile following 415nm excitation. Black lines are data, heavy lines (red, blue) are fit.

Table S2. Fitting parameters of **1** in acetonitrile following 415nm excitation.

R^2 = 0.97667

λ / nm	τ_1 / ps	A_1	τ_2 / ps	A_2	y_0
533	0.19744 ± 0.00694	-0.01068 ± 5.64e-4 (rise)	8.60555 ± 0.37342	0.00236 ± 4.02e-5 (decay)	0.0054 ± 3.92e-5
557		-0.00938 ± 5.17e-4 (rise)		9.71e-4 ± 3.90e-5 (decay)	0.00753 ± 2.64e-5

CuHETPHEN **1** in acetonitrile, cont.

Determination of τ_3 for **1** was obtained using a mono-exponential decay model to the kinetics at 451, 516, 533, and 557nm from 50-3000ps:

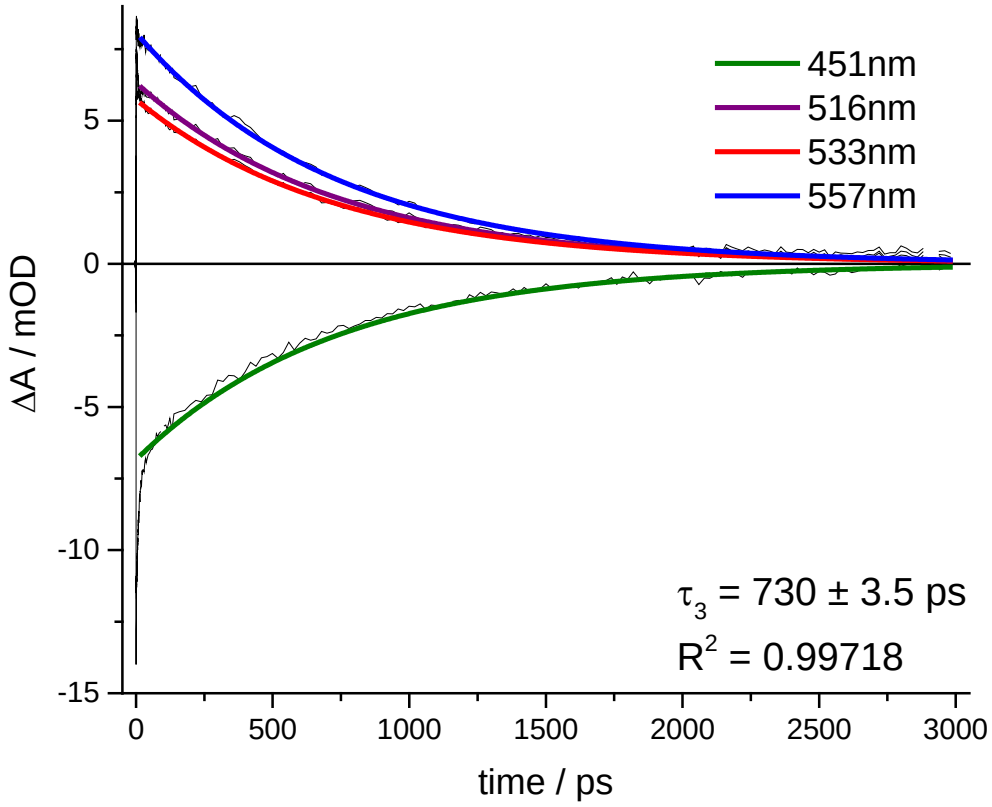

Figure S8. Global fit of ^{3}MLCT decay of **1** in acetonitrile following 415nm excitation. Black lines are data, heavy lines (green, purple, red, blue) are fit to data.

CuHETPHEN **2** in acetonitrile

Given the significant difference in magnitude, the initial kinetics (τ_1, τ_2) and ^{3}MLCT decay (τ_3) were fit separately using a global multi-exponential decay routine over multiple wavelengths (noted below). The complete ^{3}MLCT decay was obtained using a nanosecond TA experimental set-up (see next section).

Determination of τ_1 and τ_2 for **2** was obtained using a bi-exponential decay fit to the kinetics at 516, 535, and 560nm from 0.2-50ps:

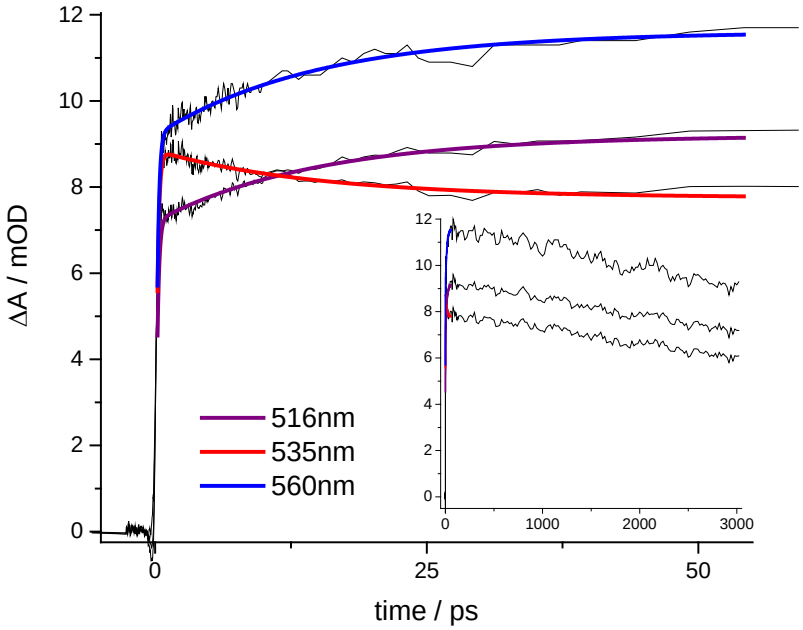

Figure S9. Global fit of early kinetics of **2** in acetonitrile following 415nm excitation. Black lines are data, heavy lines (purple, red, blue) are fit. Inset shows complete kinetics obtained from ultrafast experiment (up to 3ns).

Table S3. Fitting parameters of **2** in acetonitrile following 415nm excitation.

R^2 = 0.98086

λ / nm	τ_1 / ps	A_1	τ_2 / ps	A_2	y_0
516		-0.00969 ± 5.94e-4 (rise, 83%)		-0.002 ± 5.56e-5 (rise, 17%)	0.0092 ± 5.26e-5
535	0.17269 ± 0.0056	-0.01175 ± 7.00e-4 (rise)	14.86011 ± 0.70961	0.0011 ± 5.10e-5 (decay)	0.00776 ± 4.14e-5
560		-0.01275 ± 7.34e-4 (rise, 84%)		-0.0024 ± 5.91e-5 (rise, 16%)	0.0116 ± 5.91e-5

CuHETPHEN **3** in acetonitrile

Given the significant difference in magnitude, the initial kinetics (τ_1, τ_2) and ^{3}MLCT decay (τ_3) were fit separately using a global multi-exponential decay routine over multiple wavelengths (noted below). The complete ^{3}MLCT decay was obtained using a nanosecond TA experimental set-up (see next section).

Determination of τ_1 and τ_2 for **3** was obtained using a bi-exponential decay fit to the kinetics at 519 and 560nm from 0.2-50ps:

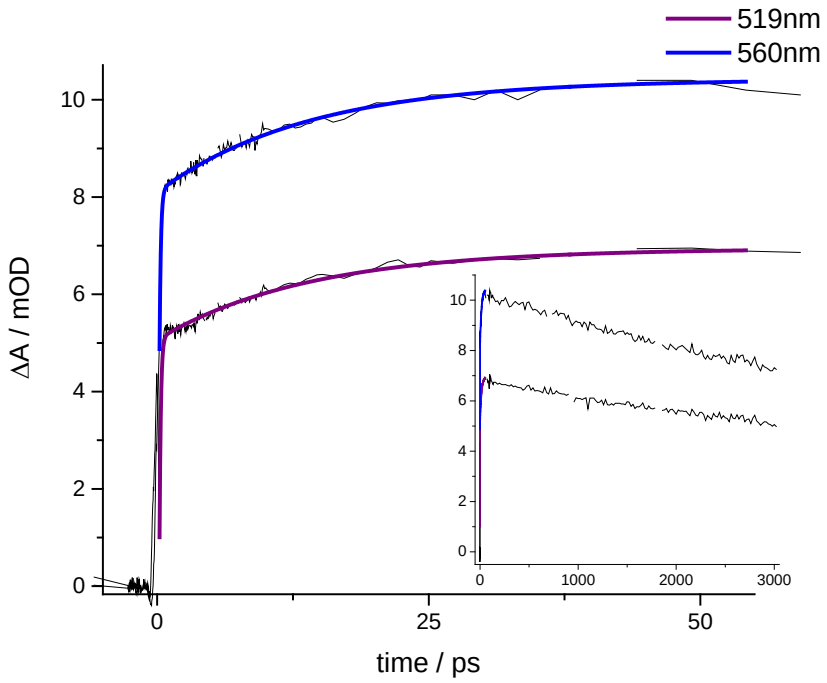

Figure S10. Global fit of early kinetics of **3** in acetonitrile following 415nm excitation. Black lines are data, heavy lines (purple, blue) are fit. Inset shows complete kinetics obtained from ultrafast experiment (up to 3ns).

Table S4. Fitting parameters of **3** in acetonitrile following 415nm excitation.

R^2 = 0.99678

λ / nm	τ_1 / ps	A_1	τ_2 / ps	A_2	y_0
519	0.11935 ± 0.00312	-0.0263 ± 0.00154 (rise, 93%)	13.967 ± 0.4967	-0.00187 ± 3.78e-5 (rise, 7%)	0.00694 ± 3.63e-5
560		-0.02097 ± 0.00125 (rise, 90%)		-0.00232 ± 4.09e-5 (rise, 10%)	0.01042 ± 4.19e-5

CuHETPHEN **4** in acetonitrile

Given the significant difference in magnitude, the initial kinetics (τ_1, τ_2) and ^{3}MLCT decay (τ_3) were fit separately using a global multi-exponential decay routine over multiple wavelengths (noted below). The complete ^{3}MLCT decay was obtained using a nanosecond TA experimental set-up (see next section).

Determination of τ_1 and τ_2 for **4** was obtained using a bi-exponential decay fit to the kinetics at 515, 532, and 552nm from 0.2-50ps:

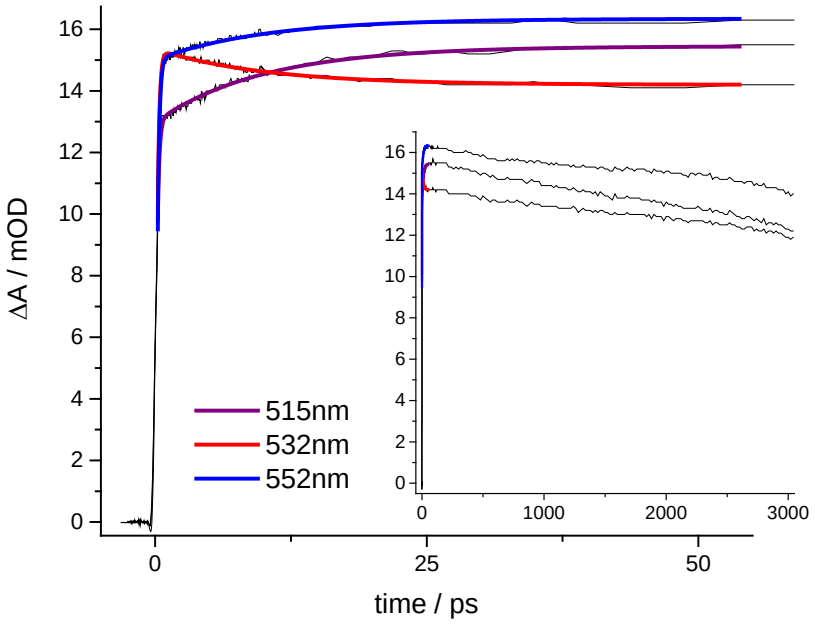

Figure S11. Global fit of early kinetics of **4** in acetonitrile following 415nm excitation. Black lines are data, heavy lines (purple, red, blue) are fit. Inset shows complete kinetics obtained from ultrafast experiment (up to 3ns).

Table S5. Fitting parameters of **4** in acetonitrile following 415nm excitation.

R^2 = 0.99035

λ / nm	τ_1 / ps	A_1	τ_2 / ps	A_2	y_0
515		-0.01357 ± 4.35e-4 (rise, 85%)		-0.00246 ± 3.203-5 (rise, 15%)	0.01545 ± 3.04e-5
532	0.16488 ± 0.00246	-0.02199 ± 6.34e-4 (rise)	9.98079 ± 0.27793	0.00117 ± 3.08e-5 (decay)	0.0142 ± 2.25e-5
552		-0.02343 ± 6.62e-4 (rise, 95%)		-0.00134 ± 3.07e-5	0.01634 ± 2.31e-5

CuHETPHEN **5** in acetonitrile

Given the significant difference in magnitude, the initial kinetics (τ_1, τ_2) and ^{3}MLCT decay (τ_3) were fit separately using a global multi-exponential decay routine over multiple wavelengths (noted below). The complete ^{3}MLCT decay was obtained using a nanosecond TA experimental set-up (see next section).

Determination of τ_1 and τ_2 for **5** was obtained using a bi-exponential decay fit to the kinetics at 580 and 597nm from 0.2-50ps:

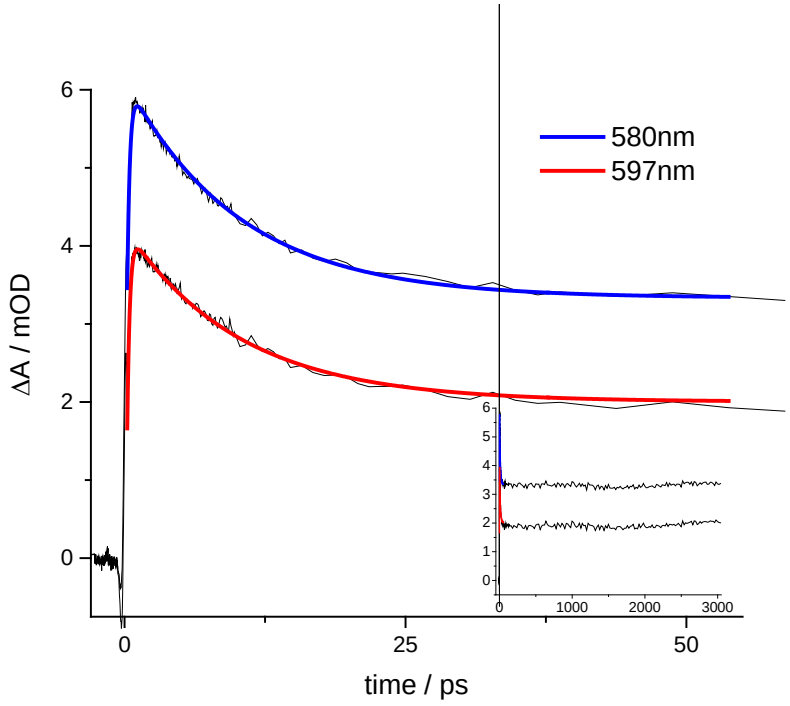

Figure S12. Global fit of early kinetics of **5** in acetonitrile following 415nm excitation. Black lines are data, heavy lines (red, blue) are fit. Inset shows complete kinetics obtained from ultrafast experiment (up to 3ns).

Table S6. Fitting parameters of **5** in acetonitrile following 415nm excitation.

R^2 = 0.99412

λ / nm	τ_1 / ps	A_1	τ_2 / ps	A_2	y_0
580	0.23234 ± 0.00602	-0.00729 ± 2.66e-4 (rise)	10.08976 ± 0.20956	0.00281 ± 2.61e-5 (decay)	0.00333 ± 2.46e-5
597		-0.00706 ± 2.61e-4 (rise)		0.00225 ± 2.56e-5 (decay)	0.002 ± 2.16e-5

Nanosecond transient optical spectra for **2**-**5**.

A nanosecond TA set-up was used to measure the complete ground state recovery and excited state decay of **2**-**5** whose lifetime is longer than the ultrafast measurements shown above.

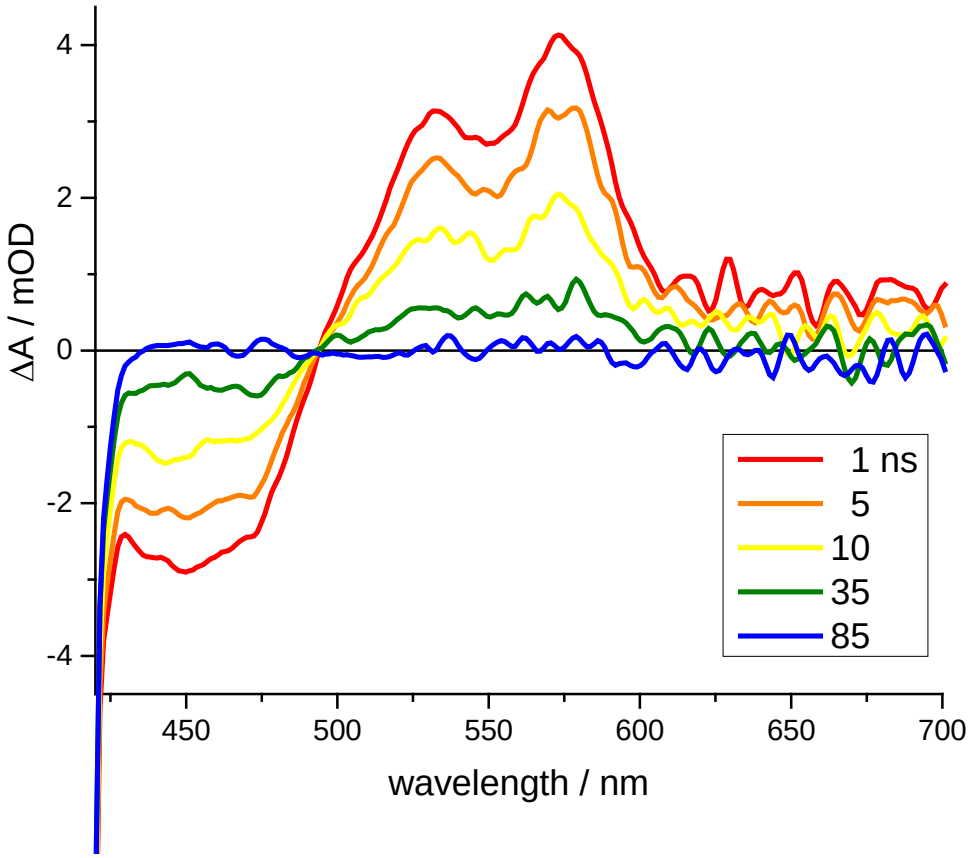

Figure S13. Nanosecond transient optical spectra of **2** in acetonitrile following 415nm excitation.

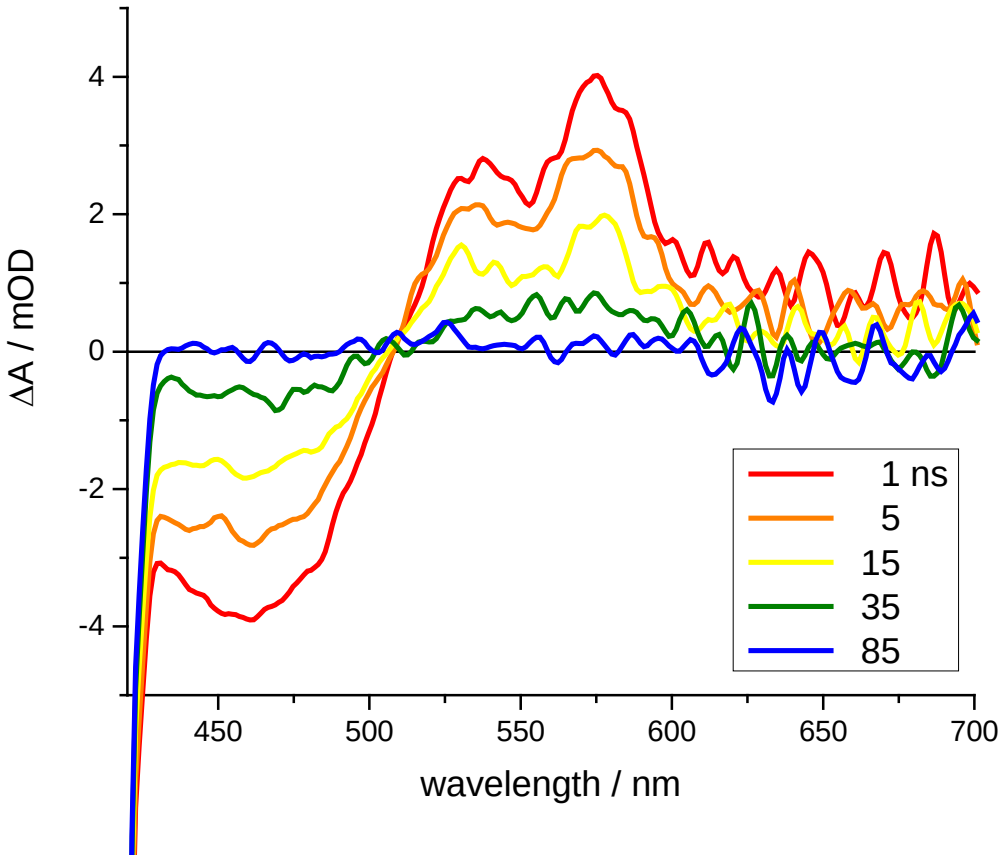

Figure S14. Nanosecond transient optical spectra of **3** in acetonitrile following 415nm excitation.

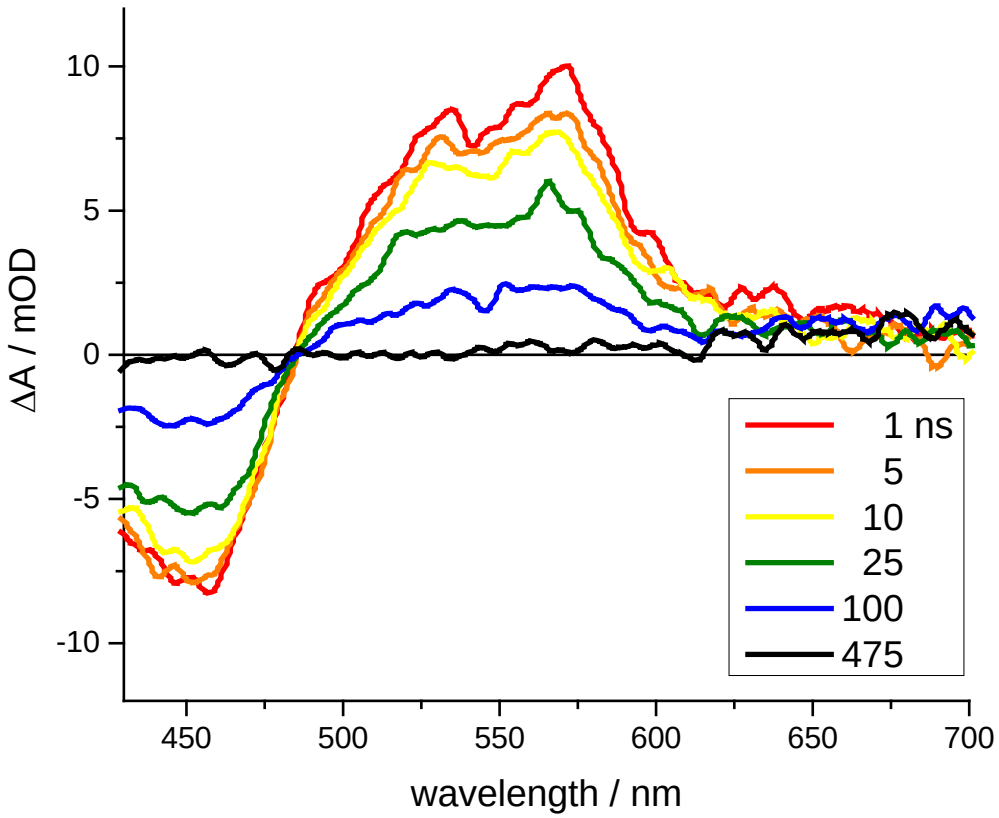

Figure S15. Nanosecond transient optical spectra of **4** in acetonitrile following 415nm excitation.

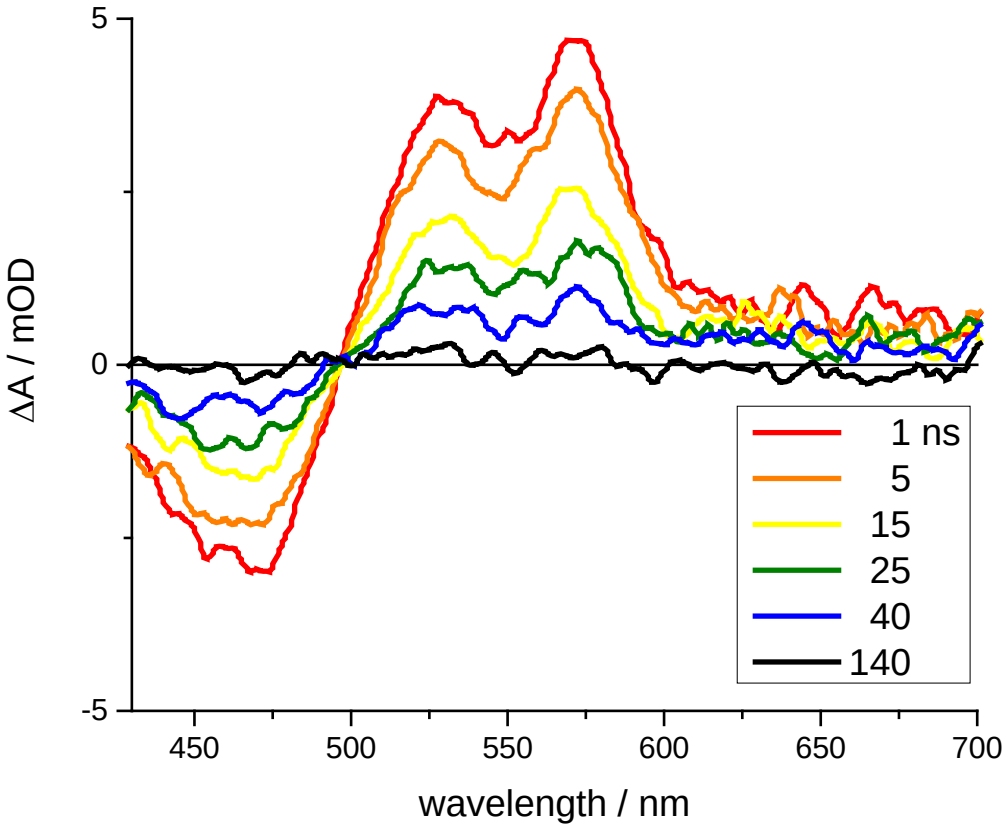

Figure S16. Nanosecond transient optical spectra of **5** in acetonitrile following 415nm excitation.

Details of fitting nanosecond kinetics for **2**-**5**.

The nanosecond kinetics for **2**-**5** were all fit by a global monoexponential decay model over several wavelengths including the ground state recovery and excited state decay.

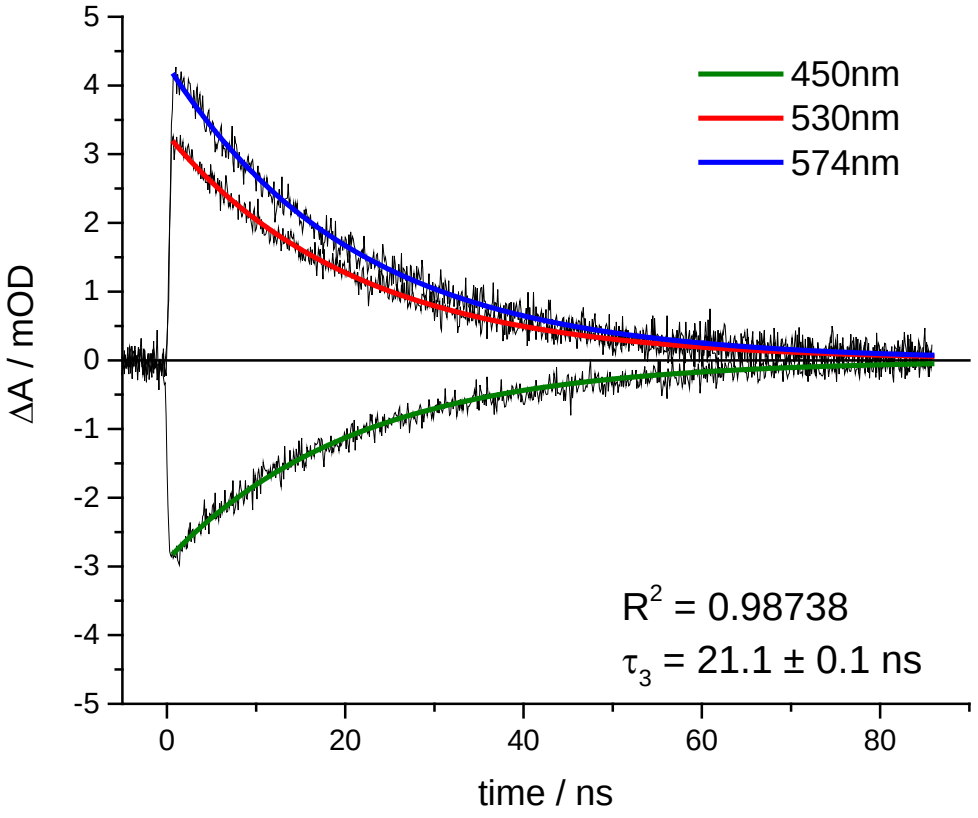

Figure S17. Selected kinetics of **2** in acetonitrile following 415nm excitation. Black lines are data, heavy lines (green, red, blue) are fit.

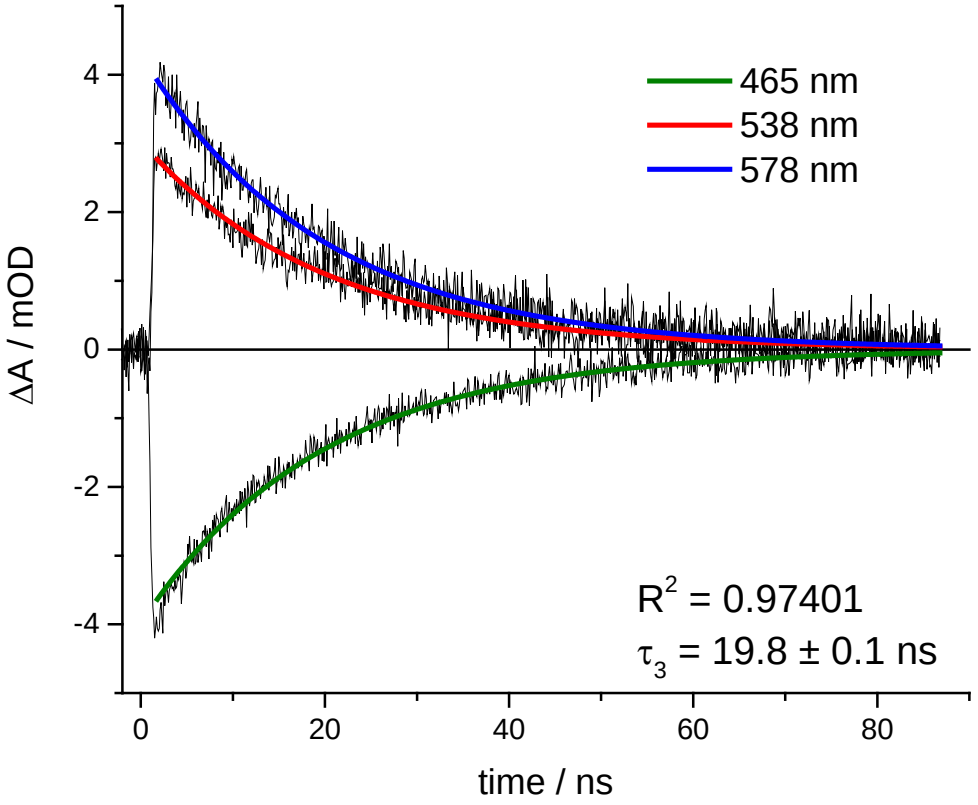

Figure S18. Selected kinetics of **3** in acetonitrile following 415nm excitation. Black lines are data, heavy lines (green, red, blue) are fit.

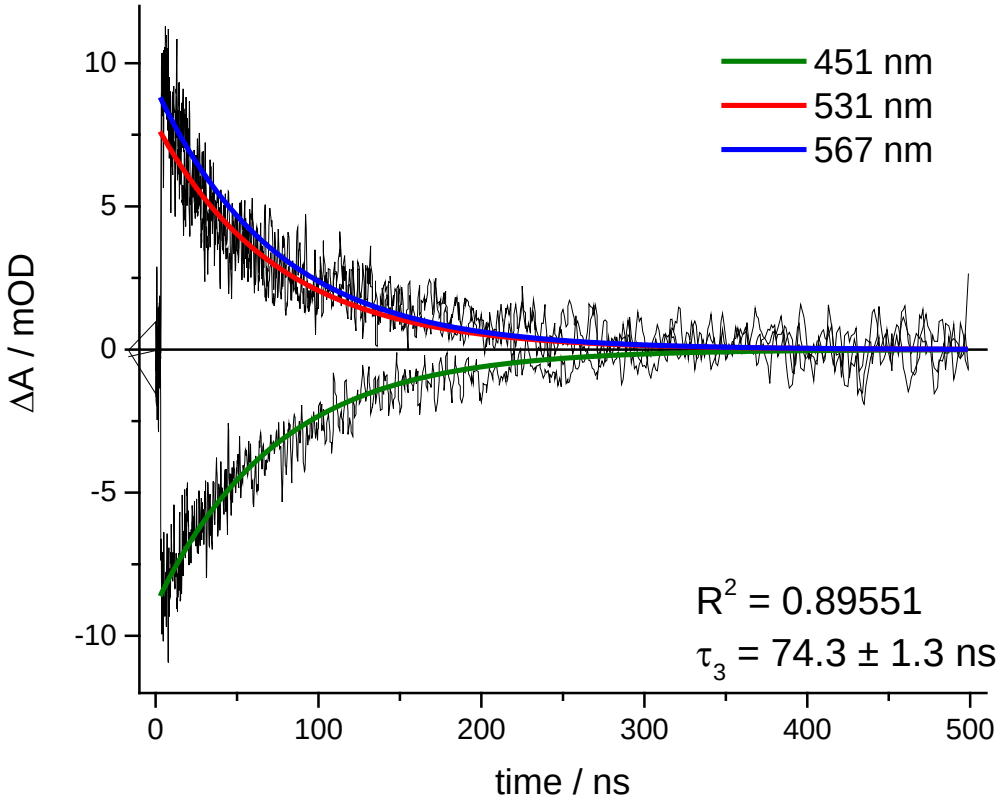

Figure S19. Selected kinetics of **4** in acetonitrile following 415nm excitation. Black lines are data, heavy lines (green, red, blue) are fit.

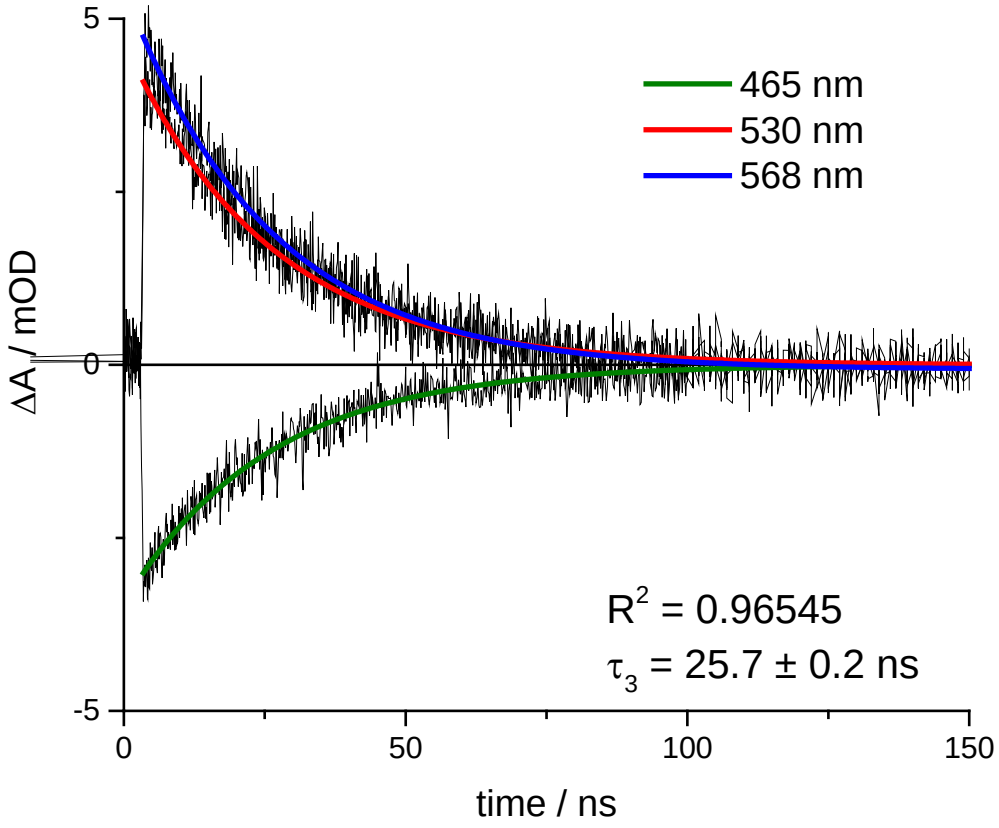

Figure S20. Selected kinetics of **5** in acetonitrile following 415nm excitation. Black lines are data, heavy lines (green, red, blue) are fit.

Transient optical spectra and kinetics of **1** and **2** in methanol.

Methanol was used for the XTA measurements since, in our experience, it generally yields a better quality jet. For the purposes of this work, the CuHETPHEN compounds have similar photophysical behavior in methanol as in acetonitrile. The transient spectra and kinetics of **1** and **2** in methanol are presented below.

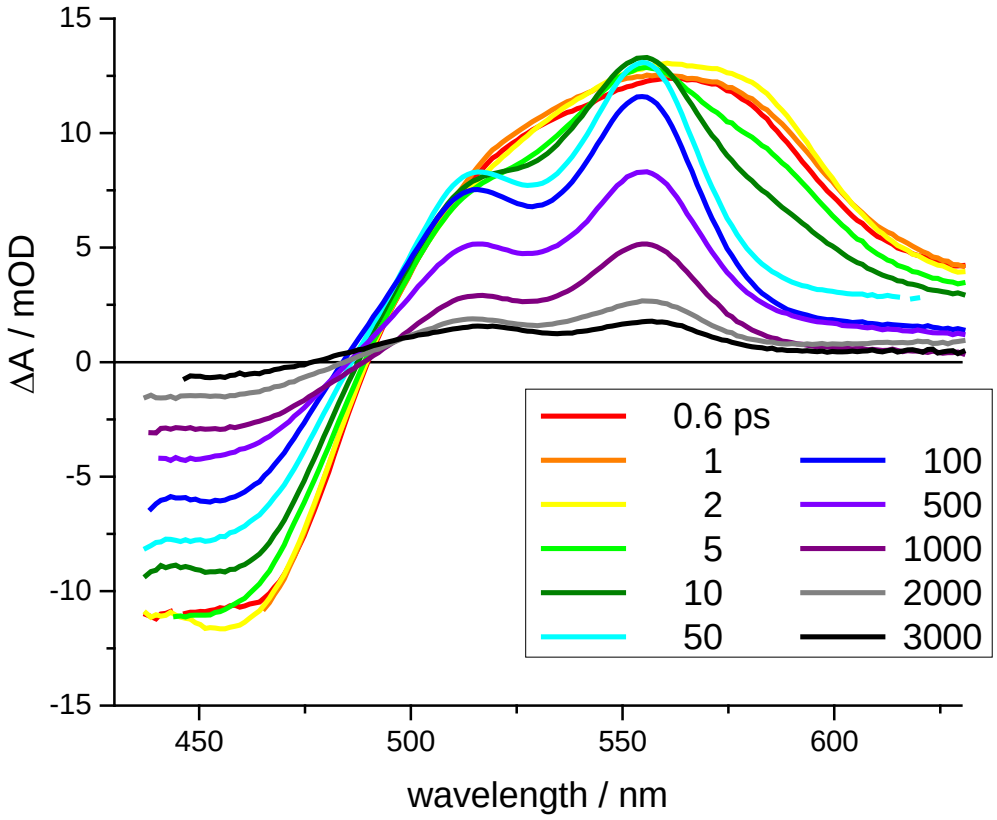

Figure S21. Transient optical spectra of **1** in methanol following 415nm excitation.

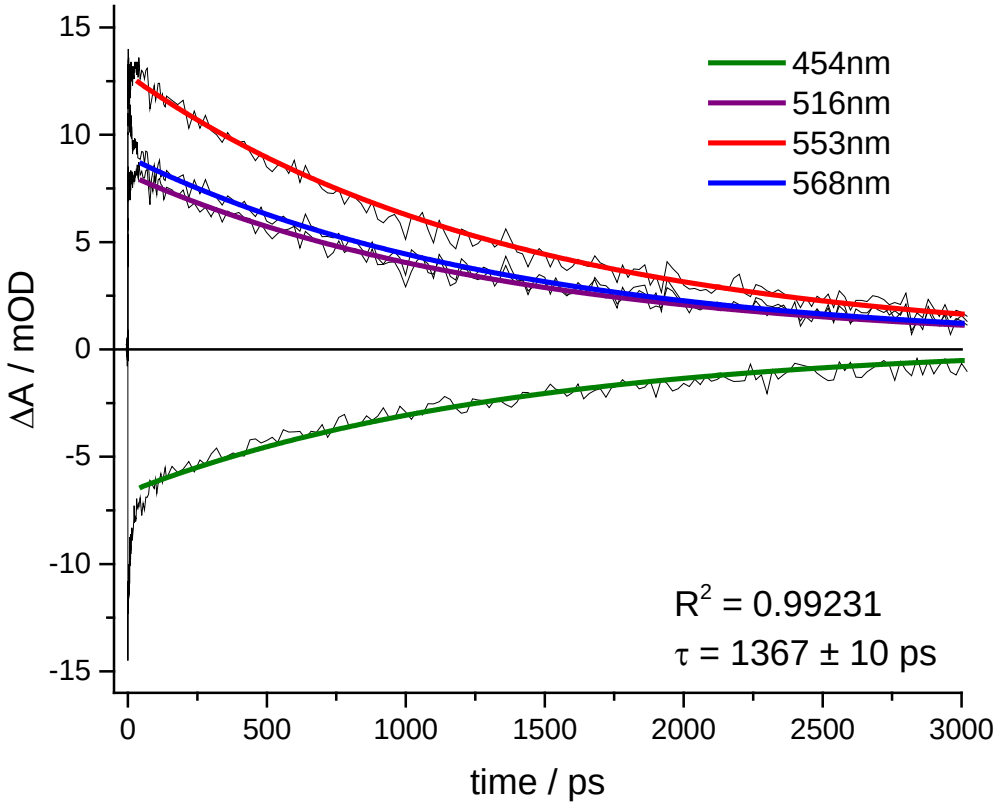

Figure S22. Global fit of ^{3}MLCT decay of **1** in methanol following 415nm excitation. Black lines are data, heavy lines (green, purple, red, blue) are fit to data.

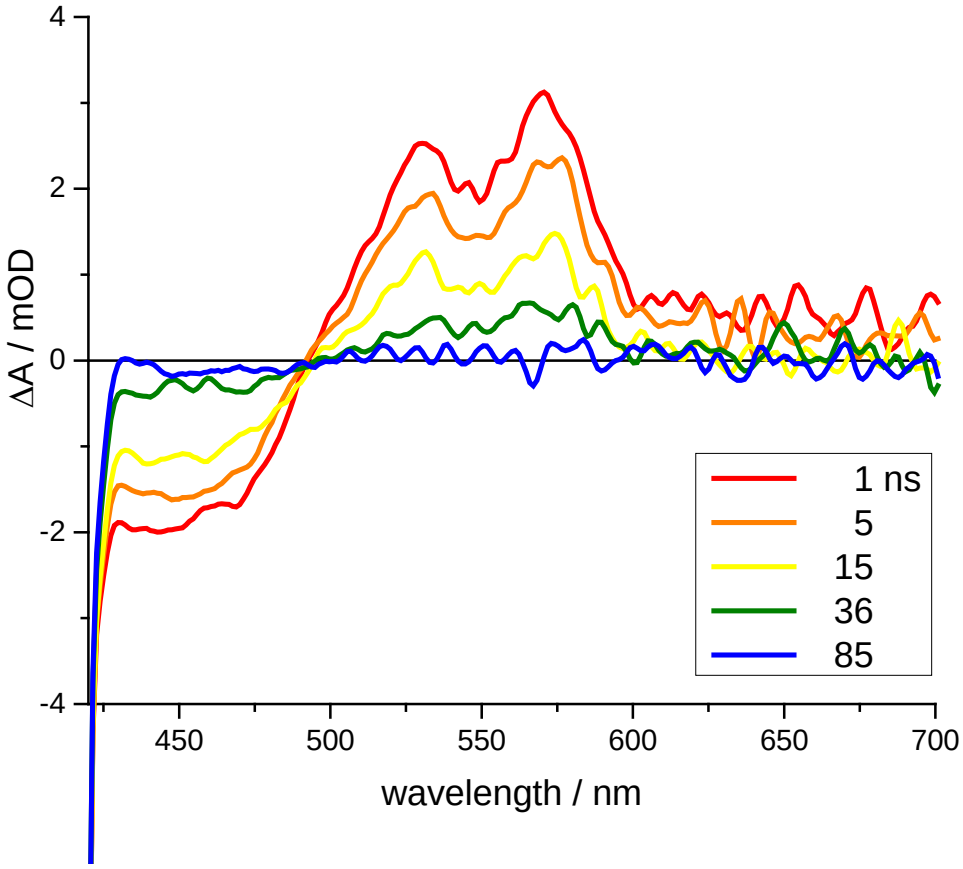

Figure S23. Nanosecond transient optical spectra of **2** in methanol following 415nm excitation.

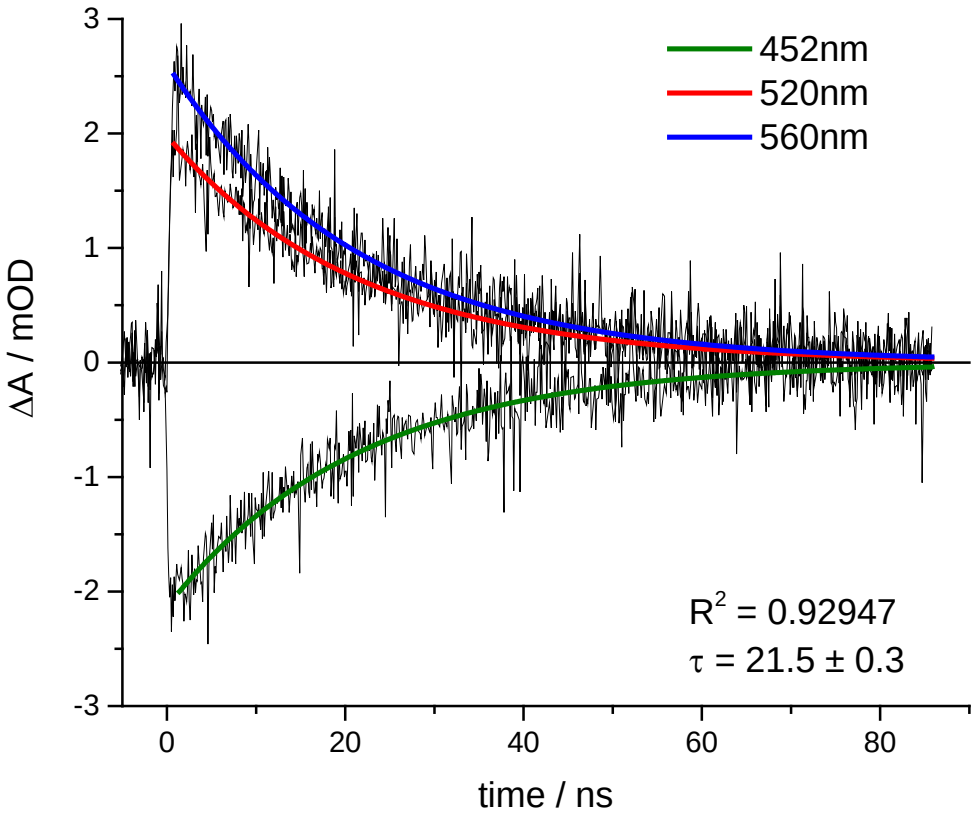

Figure S24. Selected kinetics of **2** in methanol following 415nm excitation. Black lines are data, heavy lines (green, red, blue) are fit.

Details of fitting ground and excited state XAS of **1** and **2**.

Determination of Excited State Fraction of the XAFS Spectrum

While processing XTA data, it is important to account for the fraction of ground state present in the laser-initiated spectra because 100% excitation by the pump laser is not achieved. To determine the fractions of ground state and excited state present in the laser-initiated spectrum, a linear combination analysis (LCA) of the experimental XANES spectrum using two reference spectra was performed. The reference spectra used for the LCA analysis of **1** and **2** were the corresponding ground state spectrum and the Cu(II)(mes$_2$bpy)(bpy)$^{2+}$ spectrum (Figure S25). The LCA function built into the Athena program was utilized. The percentage of the remaining ground-state in the laser-initiated spectrum was determined as 88% for **1** and 83% for **2**. The linear combination fits are shown in Figure S26.

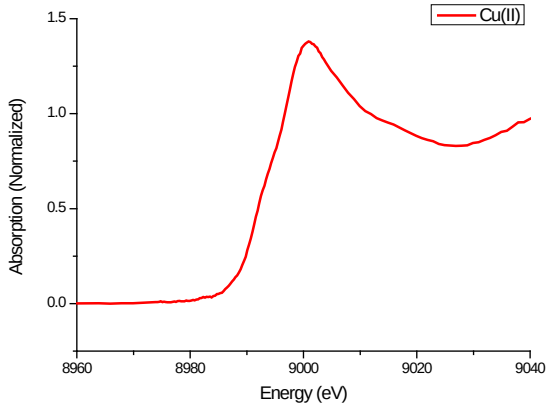

Figure S25. XANES spectrum of Cu(II)(mes$_2$bpy)(bpy)$^{2+}$ in methanol.

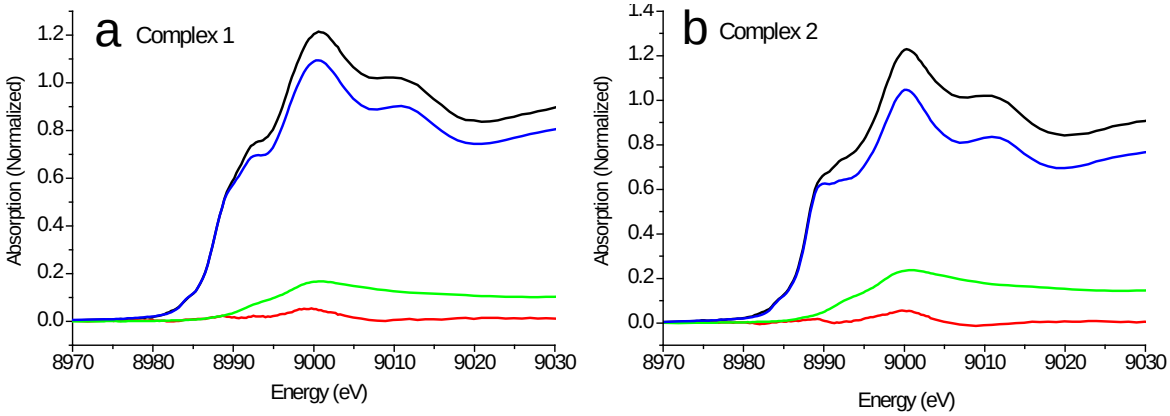

Figure S26. Linear combination fits for (a) complex **1** (88% ground state) and (b) complex **2** (83% ground state). The laser-initiated spectrum is shown in black, the ground state spectrum is in blue, the Cu(II) is in green, and the residual between the laser-initiated spectrum and the linear combination fit is shown in red.

Details of EXAFS fitting of the Ground state and Excited state

With the fractions of the ground state and the excited state determined, the ^{3}MLCT state XAFS spectra could be extracted. The ground state and ^{3}MLCT state spectra were processed and analyzed in Artemis to extract atom-atom distances. The ground-state and the ^{3}MLCT state XAFS spectra of **1** in methanol are shown in Figure S27 (k-space) and Figure S28 (R-space); the corresponding spectra for **2** in methanol are shown in Figure S29 (k-space) and S30 (R-space). All k-space spectra are plotted with a k-weight of 2. The k-space window for the Fourier transform into the R-space was chosen to maximize the number of oscillations available for fitting while minimizing the noise. The corresponding crystal structures of **1** and **2** were used as the model structures for the systems in both the ground state and ^{3}MLCT state, and the scattering paths were generated using the FEFF 6.0 program built into Artemis. The S_0^2 and ΔE parameters were set to the same values for the ground state and the excited state of each complex. While the ground state spectra had a high signal-to-noise ratio for adequate EXAFS fitting beyond the first shell, the ^{3}MLCT state spectra had a poor signal-to-noise ratio and only the first shell, the Cu – N distance, was fit. The EXAFS fitting parameters are tabulated in Table S5 and S6 for complexes **1** and **2**, respectively. The atoms used in the fitting are labeled in Figure S31. While multiple scattering paths were included, their contributions to the overall fitting were minor and only in the higher shell, hence only the single nitrogen and carbon scattering paths are described.

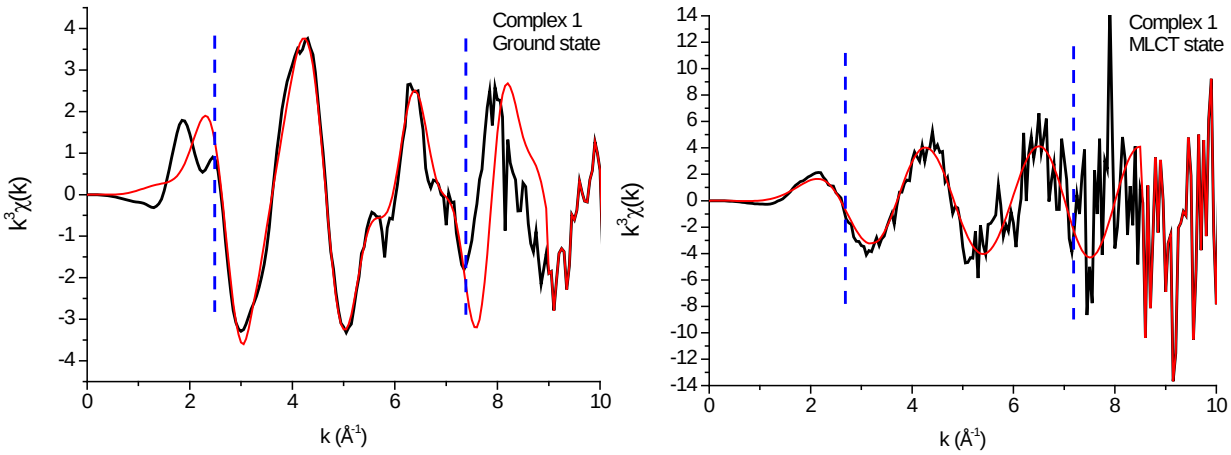

Figure S27. EXAFS spectra of **1** in ground state (left) and ^{3}MLCT state (right) in *k*-space. The black line is the experimental data and the red line is the fit. Dotted blue lines indicate the *k*-range used for Fourier transform to generate the *R*-space spectra in Figure S28. The *k*-range is 2.6 – 7.5 Å^{-1} for the ground state and 2.6 – 7.1 Å^{-1} for the ^{3}MLCT state, with a Hanning window with a width of 0.2 Å^{-1}.

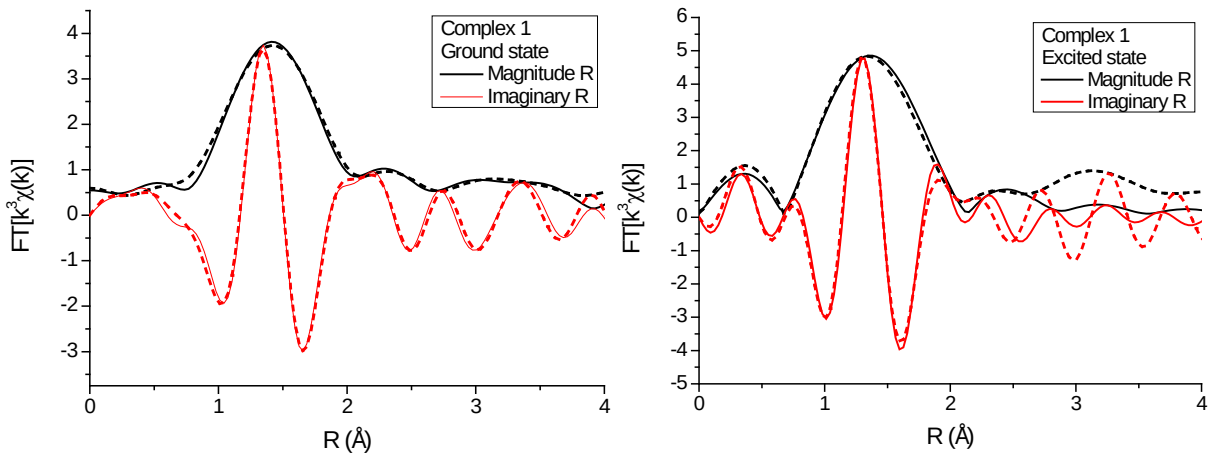

Figure S28. Fourier transform spectra in magnitude *R* (black) and imaginary *R* (red) space of **1** in the ground state (left) and MLCT state (right). The dotted line is the experimental spectrum and the solid line is the fit. The fitting range was 0.8 - 3.8 Å for the ground state and the 0.8 – 2.6 Å for the ^{3}MLCT state.

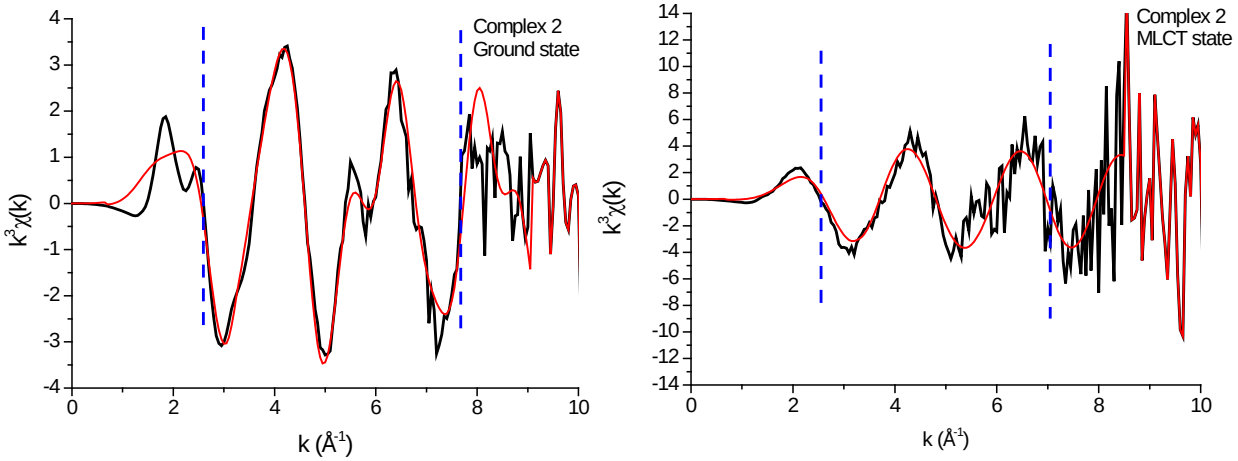

Figure S29. EXAFS spectra of **2** in ground state (left) and ^{3}MLCT state (right) in *k*-space. The black line is the experimental data and the red line is the fit. Dotted blue lines indicate the *k*-range used for Fourier transform to generate the *R*-space spectra in Figure S30. The *k*-range is 2.7 – 7.6 Å^{-1} for the ground state and 2.2 – 7.1 Å^{-1} for the ^{3}MLCT state, with a Hanning window with a width of 0.2 Å^{-1}.

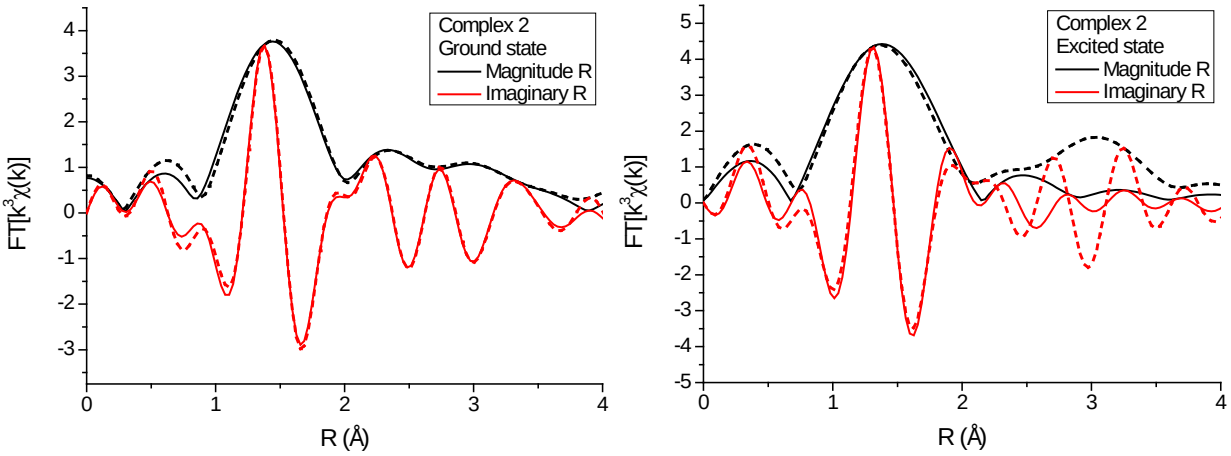

Figure S30. Fourier transform spectra in magnitude *R* (black) and imaginary *R* (red) space of complex **2** in ground state (left) and ^{3}MLCT state (right). The dotted line is the experimental spectrum and the solid line is the fit. The fitting range was 0.8 - 3.8 Å for the ground state and the 0.8 – 2.2 Å for the ^{3}MLCT state.

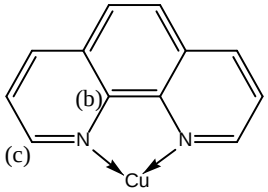

Figure S31. Atomic centers used in EXAFS data fitting.

Table S5. Fitting Parameters of **1**.

ΔE = 0.66 eV, S_o^2 = 1.0				
Atom-atom scattering path	Atom-atom distance (Å, ±0.02 Å)		Debye-Waller factor (Å^2, ±0.001 Å^2)	
	Ground state	Excited state	Ground state	Excited state
Cu – N (CN[a] = 4)	1.98	1.95	0.0075	0.0026
Cu – C (b) (CN = 4)	2.75	-	0.0082	-
Cu – C (c) (CN = 4)	3.05	-	0.0090	-

[a] Coordination number

Table S6. Fitting Parameters of **2**.

ΔE = 1.81 eV, S_o^2 = 1.0				
Atom-atom scattering path	Atom-atom distance (Å, ±0.02 Å)		Debye-Waller factor (Å^2, ±0.001 Å^2)	
	Ground state	Excited state	Ground state	Excited state
Cu – N (CN[a] = 4)	2.01	1.96	0.0081	0.0039
Cu – C (b) (CN = 4)	2.82	-	0.0090	-
Cu – C (c) (CN = 4)	3.12	-	0.0079	-

[a] Coordination number

The temporal resolution of the X-ray transient absorption measurement is ~50 ps, so it cannot be used to determine the ultrafast internal conversion or intersystem crossing rates, which are on the order of 200fs and 10ps, respectively. However, the relaxation rates from the ^{3}MLCT state, τ_3, were determined from optical transient absorption to be 1.4ns and 21.5ns in methanol for complexes **1** and **2**, respectively, making them good candidates for determination by XTA as well. The time trace for complex **1** taken at the $1s \rightarrow 4p_z$ transition peak at 8993 eV is given in Figure S32, showing a recovery of the bleach observed at this energy on the timescale of a few nanoseconds. The trace was fit to the sum of a single exponential decay and a constant offset, multiplied by an error function to account for the instrument response. The fit, shown as a black trace in Figure S32, gives a τ_3 value of 1.3 ± 0.1ns, in excellent agreement with the relaxation time measured by OTA, and an instrument response of 50 ± 5ps.

Electrical noise from the firing of the Pockels cells in the Ti:Sapph regenerative amplifier appears in the traces on the oscilloscope from the avalanche photodiodes that measure the X-ray fluorescence from the sample, resulting in large oscillations that dominate the time traces at delay times beyond a few nanoseconds. The onset of this noise is clear in Figure S32, beginning at ~1.5ns. This simply results in a constant offset between the laser-on and laser-off spectra taken at a fixed delay time, and thus does not impact the comparison of the ground state and laser initiated XANES or EXAFS spectra. However, the Pockels cell noise was too strong to allow us to fit the longer relaxation time of complex **2**.

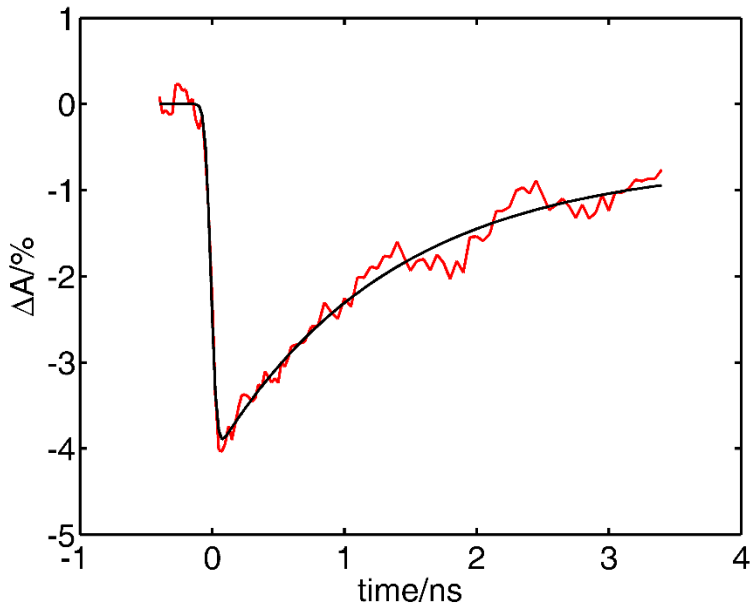

Figure S32. Time trace for **1** taken at the $1s \rightarrow 4p_z$ transition peak at 8993 eV (red) and a fit of the data (black).